A new high-order nine-point stencil, based on integrated-RBF approximations, for the first biharmonic equation

N. Mai-Duy[1,*], D. Strunin[2] and W. Karunasena[1]
[1] School of Engineering,
[2] School of Mathematics, Physics and Computing,
University of Southern Queensland, Toowoomba, QLD 4350, Australia

Submitted to *Engineering Analysis with Boundary Elements*, March 2022; revised, June 2022

Abstract This paper is concerned with the development of a new compact 9-point stencil, based on integrated-radial-basis-function (IRBF) approximations, for the discretisation of the first biharmonic equation in two dimensions. Derivatives of not only the first order but also the second order and higher are included in the approximations on the stencil. These nodal derivative values, except for the boundary values of the derivative, are directly derived from nodal variable values along the grid lines rather than from the biharmonic equation, and they are updated through iteration. With these features, the double boundary conditions are imposed in a proper way. The biharmonic equation is enforced at grid points near the boundary without any special treatments. More importantly, they enable the IRBF solution to be highly accurate and not influenced by the RBF width. There is no need for searching the optimal value of the RBF width. The proposed stencil can be used to solve the biharmonic problem defined on a rectangular/non-rectangular domain. A fast convergence rate with respect to grid refinement (up to ten) is achieved.

Keywords: first biharmonic equation, double boundary conditions, non-coupled approach,

*Corresponding author E-mail: nam.mai-duy@usq.edu.au, Telephone +61-7-46312748, Fax +61-7-46312529

compact stencils, integrated radial basis functions

1 Introduction

The biharmonic equation arises in the mathematical modelling of many problems in engineering and science such as the deformation of a thin plate and the flow of a fluid. There are two types of biharmonic problems. For the second biharmonic problem, along the boundary, the field variable and its second normal derivative are given. The problem can be converted into the Dirichlet problems for two Poisson equations that are solved separately. For the first biharmonic problem, along the boundary, the field variable and its first normal derivative are given. Numerically solving the first biharmonic equation faces some significant challenges, namely the approximation of high-order derivatives and cross derivatives, and the imposition of double boundary conditions. Various numerical schemes have been developed, e.g., [1,2,3,4,5,6,7]. In the context of finite difference methods [1], the standard 13-point stencil with truncation error of $O(h^2)$ and the 25-point (5×5) approximation with truncation error of $O(h^4)$ are obtained, where some grid points outside the problem domain are required. Approximations at these fictitious points are carried out to impose the boundary values of the derivative. It was found in [8] that the boundary approximations used can strongly affect the accuracy of the numerical solution. One way to avoid the fictitious points is to use the 9-point (3×3) stencil reported in [9], where the field variable and its first derivative are considered as unknowns in the interpolation system (three unknown values at each grid node for the formula with $O(h^4)$). This approach results in a much larger system of algebraic equations (27 unknowns in each equation while there are only 13 unknowns in each equation for the second order method). With regard to the calculation of high-order derivatives, special attention is required as the approximation of derivatives of higher order has larger errors. The use of higher-order conventional Lagrange polynomials does not guarantee to yield a better quality (smoothness) of approximation.

The radial basis functions (RBFs) methods have been widely used in solving partial dif-

ferential equations (PDEs), e.g., [10,11,12,13,14,15,16]. The RBF approximations can be constructed through differentiation (DRBF) or integration (IRBF). In the early IRBF works (e.g. [17,18,19,20]), the methods are based on global approximations that involve only the nodal values of the field variable. The RBF methods are a kind of high-order discretisation scheme and can work well with unstructured points. Some RBFs such as the multiquadric function involve the shape parameter or the RBF width that can strongly affect the solution accuracy. Choosing an optimal value of the RBF width is a difficult task. Since integration improves smoothness, the IRBF approach is more suitable for approximating high-order derivatives. In addition, with the presence of integration constants, there are more unknown coefficients in the interpolation system and some extra equations can thus be added. This provides an effective way of implementing double boundary conditions and constructing compact stencils that involve the nodal values of both the field variable and its derivatives. In this paper, we propose new IRBF approximations using only the nine grid points for solving the first biharmonic equation. The construction of the proposed stencil is based on 3-point approximations recently developed for solving second-order PDEs in [21,22]. Nodal values of the first-order derivatives and higher ones along the grid lines are included in the IRBF approximations. These derivative values are directly derived from the nodal values of the field variable and updated through iteration. In this regard, the proposed stencil is not dependent on the governing equation, and there are only 9 unknowns in each equation. No modifications are needed at grid points adjacent to the boundary, in marked contrast to special treatments required in the standard 13-point and 25-point stencils. The proposed approach enables the boundary values of the derivative to be exactly satisfied, and the IRBF solution to be highly accurate and not influenced by the RBF width. It is found that the latter is achieved by simply employing an IRBF scheme of high order (i.e. ≥ 6) on the stencil. There is no need for searching the optimal value of the RBF width. We note some recent RBF works (e.g. [23]) concerning the use of polyharmonic splines with augmented polynomials to overcome the issue of the RBF width. Like the polyharmonic-spline-based methods, the proposed approximations also involve some polynomials of high order. However, these polynomials are produced from the integration of the RBFs. Unlike the polyharmonic-spline-based methods, the nodal values of the derivatives along the grid

lines are incorporated into the IRBF approximations to form the determined interpolation system.

The remaining of the paper is organised as follows. Section 2 is about the first biharmonic equation. The proposed 9-point stencil is presented in Section 3 and numerically verified in Section 4. Section 5 gives some concluding remarks.

2 Governing equations

Consider the first biharmonic problem governed by

$$\frac{\partial^4 u}{\partial x^4} + 2\frac{\partial^4 u}{\partial x^2 \partial y^2} + \frac{\partial^4 u}{\partial y^4} = b(x,y), \quad (x,y) \in \Omega, \tag{1}$$

with the boundary conditions

$$u = g_1(x,y), \quad \frac{\partial u}{\partial n} = g_2(x,y), \quad (x,y) \in \partial\Omega, \tag{2}$$

where Ω is a rectangular domain, $\partial\Omega$ is its boundaries, $\partial u/\partial n$ represents the outward normal on $\partial\Omega$, and $b(x,y)$, $g_1(x,y)$ and $g_2(x,y)$ are some given functions.

Equation (1) is equivalent to a set of two coupled Poisson equations for u and v

$$\frac{\partial^2 u}{\partial x^2} + \frac{\partial^2 u}{\partial y^2} = v, \tag{3}$$

$$\frac{\partial^2 v}{\partial x^2} + \frac{\partial^2 v}{\partial y^2} = b. \tag{4}$$

Numerically solving equation (1) involves the discretisation of fourth-order derivatives and cross/mixed derivatives, while numerically solving equations (3) and (4) involves the discretisation of second-order derivatives only.

In this work, we discretise the biharmonic equation in the form of a coupled system of (3)

and (4) for which only second derivatives are approximated. However, in discretisation form, the nodal values of v are replaced with the nodal values of u through (3), resulting in the final algebraic equation set that contains only the nodal values of the variable u. Thus, the non-coupled approach is actually employed here to solve the first biharmonic problem.

3 Proposed stencil

We first present the proposed stencil for the case of rectangular domain. An N_x-by-N_y Cartesian grid is employed to represent the problem domain. The proposed stencil uses only the 9 grid nodes on which the approximations are built from one dimensional 3-point approximations. The 3-point approximations in the x and y directions are constructed separately. When compared to [24], where nodal PDE values are taken as extra information, the sizes of the present interpolation matrices are much smaller.

3.1 3-point approximations

Let η represent the independent variable x and y, and f the dependent variable u and v. Consider 3 grid points $(\eta_{i-1}, \eta_i, \eta_{i+1})$, over which the variable f can be represented by an

IRBF approximation scheme

$$\frac{\partial^q f(\eta)}{\partial \eta^q} = \sum_{i=1}^{3} w_i G_i(\eta) = \sum_{i=1}^{3} w_i I_i^{(q)}(\eta), \tag{5}$$

$$\frac{\partial^{q-1} f(\eta)}{\partial \eta^{q-1}} = \sum_{i=1}^{3} w_i I_i^{(q-1)}(\eta) + c_1, \tag{6}$$

$$\frac{\partial^{q-2} f(\eta)}{\partial \eta^{q-2}} = \sum_{i=1}^{3} w_i I_i^{(q-2)}(\eta) + c_1\eta + c_2, \tag{7}$$

$$\cdots \quad \cdots \quad \cdots$$

$$\frac{\partial f(\eta)}{\partial x} = \sum_{i=1}^{3} w_i I_i^{(1)}(\eta) + c_1 \frac{\eta^{q-2}}{(q-2)!} + c_2 \frac{\eta^{q-3}}{(q-3)!} + \cdots + c_{q-1}, \tag{8}$$

$$f(\eta) = \sum_{i=1}^{3} w_i I_i^{(0)}(\eta) + c_1 \frac{\eta^{q-1}}{(q-1)!} + c_2 \frac{\eta^{q-2}}{(q-2)!} + \cdots + c_{q-1}\eta + c_q, \tag{9}$$

where $G_i(\eta)$ is the RBF, $I_i^{(q-1)}(\eta) = \int I_i^{(q)}(\eta)d\eta$, $I_i^{(q-2)}(\eta) = \int I_i^{(q-1)}(\eta)d\eta$, $\cdots$, $I_i^{(0)}(\eta) = \int I_i^{(1)}(\eta)d\eta$, (w_1, w_2, w_3) the RBF coefficients, and $(c_1, c_2, \cdots, c_q)$ the integration constants. For the multiquadric function, $G_i(\eta) = \sqrt{(\eta - \eta_i)^2 + a_i^2}$, where a is the width/shape-parameter. In (5)-(9), RBFs are used to represent the qth order derivative and we refer it to as an IRBF scheme of order q, denoted by IRBFq. The analytical IRBF forms are shown in the Appendix.

For an IRBFq, the presence of q integration constants enables the addition of q extra equations to the conversion of the RBF space into the physical space. We utilise these equations to impose derivatives at the two end-nodes: the first-, $\cdots$, and the $\left(\frac{q}{2}\right)$th-order derivatives for equation (3) and the second-, $\cdots$, and the $\left(\frac{q}{2}+1\right)$th-order derivatives for equation (4).

For equation (3), the conversion system is constructed as follows

$$\widehat{u} = \mathcal{C}_u \widehat{w}_u, \tag{10}$$

where

$$\widehat{u} = \left(u_{i-1}, u_i, u_{i+1}, \frac{\partial u_{i-1}}{\partial \eta}, \frac{\partial u_{i+1}}{\partial \eta}, \cdots, \frac{\partial^{q/2} u_{i-1}}{\partial \eta^{q/2}}, \frac{\partial^{q/2} u_{i+1}}{\partial \eta^{q/2}}\right)^T,$$

$$\widehat{w}_u = \left(w_1, w_2, w_3, c_1, \cdots, c_q\right)^T,$$

and

$$\mathcal{C}_u = \begin{bmatrix} I_1^{(0)}(\eta_{i-1}) & I_3^{(0)}(\eta_{i-1}) & I_3^{(0)}(\eta_{i-1}) & \frac{\eta_{i-1}^{q-1}}{(q-1)!} & \cdots & \eta_{i-1} & 1 \\ I_1^{(0)}(\eta_i) & I_3^{(0)}(\eta_i) & I_3^{(0)}(\eta_i) & \frac{\eta_i^{q-1}}{(q-1)!} & \cdots & \eta_i & 1 \\ I_1^{(0)}(\eta_{i+1}) & I_3^{(0)}(\eta_{i+1}) & I_3^{(0)}(\eta_{i+1}) & \frac{\eta_{i+1}^{q-1}}{(q-1)!} & \cdots & \eta_{i+1} & 1 \\ I_1^{(1)}(\eta_{i-1}) & I_3^{(1)}(\eta_{i-1}) & I_3^{(1)}(\eta_{i-1}) & \frac{\eta_{i-1}^{q-2}}{(q-2)!} & \cdots & 1 & 0 \\ I_1^{(1)}(\eta_{i+1}) & I_3^{(1)}(\eta_{i+1}) & I_3^{(1)}(\eta_{i+1}) & \frac{\eta_{i+1}^{q-2}}{(q-2)!} & \cdots & 1 & 0 \\ \cdots & \cdots & \cdots & & \cdots & & \\ I_1^{(q/2)}(\eta_{i-1}) & I_3^{(q/2)}(\eta_{i-1}) & I_3^{(q/2)}(\eta_{i-1}) & \frac{\eta_{i-1}^{q/2-1}}{(q/2-1)!} & \cdots & 0 & 0 \\ I_1^{(q/2)}(\eta_{i+1}) & I_3^{(q/2)}(\eta_{i+1}) & I_3^{(q/2)}(\eta_{i+1}) & \frac{\eta_{i+1}^{q/2-1}}{(q/2-1)!} & \cdots & 0 & 0 \end{bmatrix}.$$

Solving (10) yields

$$\widehat{w}_u = \mathcal{C}_u^{-1}\widehat{u}. \tag{11}$$

Thus, the second derivative of u at η_i is calculated by

$$\frac{\partial^2 u_i}{\partial \eta^2} = \mathcal{D}_{2u\eta}^{[q]}\widehat{u}, \tag{12}$$

where $\mathcal{D}_{2u\eta}^{[2]} = \begin{bmatrix} I_1^{(2)}(\eta_i) & I_2^{(2)}(\eta_i) & I_3^{(2)}(\eta_i) & \frac{\eta_i^{q-3}}{(q-3)!} & \cdots & 0 \end{bmatrix}\mathcal{C}_u^{-1}$. It is noted that $\mathcal{D}_{2u\eta}^{[q]}$ is a row matrix of the $(q+3)$ coefficients by the qth-order IRBF scheme. In practice, the coefficient set $\mathcal{D}_{2u\eta}^{[q]}$ is obtained by using Gaussian elimination to solve the following algebraic equation set:

$$\mathcal{C}_u^T \mathcal{D}_{2u\eta}^{[q]^T} = \left(I_1^{(2)}(\eta_i), I_2^{(2)}(\eta_i), I_3^{(2)}(\eta_i), \frac{\eta_i^{q-3}}{(q-3)!} \cdots, 0 \right)^T. \tag{13}$$

For equation (4), the conversion system is constructed as follows

$$\widehat{v} = \mathcal{C}_v \widehat{w}_v, \tag{14}$$

where

$$\widehat{v} = \left(v_{i-1}, v_i, v_{i+1}, \frac{\partial^2 v_{i-1}}{\partial \eta^2}, \frac{\partial^2 v_{i+1}}{\partial \eta^2}, \cdots, \frac{\partial^{q/2+1} v_{i-1}}{\partial \eta^{q/2+1}}, \frac{\partial^{q/2+1} v_{i+1}}{\partial \eta^{q/2+1}} \right)^T,$$

$$\widehat{w}_v = \left(w_1, w_2, w_3, c_1, \cdots, c_q \right)^T,$$

and

$$\mathcal{C}_v = \begin{bmatrix} I_1^{(0)}(\eta_{i-1}) & I_3^{(0)}(\eta_{i-1}) & I_3^{(0)}(\eta_{i-1}) & \frac{\eta_{i-1}^{q-1}}{(q-1)!} & \cdots & \eta_{i-1} & 1 \\ I_1^{(0)}(\eta_i) & I_3^{(0)}(\eta_i) & I_3^{(0)}(\eta_i) & \frac{\eta_i^{q-1}}{(q-1)!} & \cdots & \eta_i & 1 \\ I_1^{(0)}(\eta_{i+1}) & I_3^{(0)}(\eta_{i+1}) & I_3^{(0)}(\eta_{i+1}) & \frac{\eta_{i+1}^{q-1}}{(q-1)!} & \cdots & \eta_{i+1} & 1 \\ I_1^{(2)}(\eta_{i-1}) & I_3^{(2)}(\eta_{i-1}) & I_3^{(2)}(\eta_{i-1}) & \frac{\eta_{i-1}^{q-3}}{(q-3)!} & \cdots & 0 & 0 \\ I_1^{(2)}(\eta_{i+1}) & I_3^{(2)}(\eta_{i+1}) & I_3^{(2)}(\eta_{i+1}) & \frac{\eta_{i+1}^{q-3}}{(q-3)!} & \cdots & 0 & 0 \\ \cdots & \cdots & \cdots & & \cdots & & \\ I_1^{(q/2+1)}(\eta_{i-1}) & I_3^{(q/2+1)}(\eta_{i-1}) & I_3^{(q/2+1)}(\eta_{i-1}) & \frac{\eta_{i-1}^{q/2-2}}{(q/2-2)!} & \cdots & 0 & 0 \\ I_1^{(q/2+1)}(\eta_{i+1}) & I_3^{(q/2+1)}(\eta_{i+1}) & I_3^{(q/2+1)}(\eta_{i+1}) & \frac{\eta_{i+1}^{q/2-2}}{(q/2-2)!} & \cdots & 0 & 0 \end{bmatrix}.$$

Solving (14) yields

$$\widehat{w}_v = \mathcal{C}_v^{-1}\widehat{v}. \tag{15}$$

Thus, the second derivative of v at η_i is calculated by

$$\frac{\partial^2 v_i}{\partial \eta^2} = \mathcal{D}_{2v\eta}^{[q]}\widehat{v}, \tag{16}$$

where $\mathcal{D}_{2v\eta}^{[q]} = \begin{bmatrix} I_1^{(2)}(\eta_i) & I_2^{(2)}(\eta_i) & I_3^{(2)}(\eta_i) & \frac{\eta_i^{q-3}}{(q-3)!} & \cdots & 0 \end{bmatrix}\mathcal{C}_v^{-1}$. It is noted that $\mathcal{D}_{2v\eta}^{[q]}$ is a row matrix of the $(q+3)$ coefficients by the qth IRBF scheme. In practice, the coefficient set $\mathcal{D}_{2v\eta}^{[q]}$ is acquired by using Gaussian elimination to solve the following algebraic equation set:

$$\mathcal{C}_v^T \mathcal{D}_{2v\eta}^{[q]^T} = \left(I_1^{(2)}(\eta_i), I_2^{(2)}(\eta_i), I_3^{(2)}(\eta_i), \frac{\eta_i^{q-3}}{(q-3)!}, \cdots, 0 \right)^T. \tag{17}$$

The row matrices $\mathcal{D}_{2u\eta}^{[q]}$ and $\mathcal{D}_{2v\eta}^{[q]}$ are all obtained numerically. There is no difference in handling between uniformly and non-uniformly distributed grid points. The conversion systems for $q = (2, 4, 6, 8)$ are shown in the Appendix.

3.2 9-point (3×3) approximations

Consider an interior node and its associated eight neighbouring nodes. They are locally numbered from bottom to top and from left to right (Figure 1). Enforcing equation (4) at the central node yields

$$\frac{\partial^2 v_5}{\partial x^2} + \frac{\partial^2 v_5}{\partial y^2} = b_5. \tag{18}$$

Making use of an IRBF scheme of order q, the left-side terms of (18) are approximated as

$$\begin{aligned}\frac{\partial^2 v_5}{\partial x^2} &= \mathcal{D}^{[q]}_{2vx}(1)v_2 + \mathcal{D}^{[q]}_{2vx}(2)v_5 + \mathcal{D}^{[q]}_{2vx}(3)v_8 + \\ &\left[\mathcal{D}^{[q]}_{2vx}(4)\frac{\partial^2 v_2}{\partial x^2} + \mathcal{D}^{[q]}_{2vx}(5)\frac{\partial^2 v_8}{\partial x^2} + \cdots + \mathcal{D}^{[q]}_{2vx}(q+2)\frac{\partial^{q/2+1} v_2}{\partial x^{q/2+1}} + \mathcal{D}^{[q]}_{2vx}(q+3)\frac{\partial^{q/2+1} v_8}{\partial x^{q/2+1}}\right], \\ &= \mathcal{D}^{[q]}_{2vx}(1)v_2 + \mathcal{D}^{[q]}_{2vx}(2)v_5 + \mathcal{D}^{[q]}_{2vx}(3)v_8 + R^{[q]}_{2vx}, \end{aligned} \tag{19}$$

where $\mathcal{D}^{[q]}_{2vx}(k)$, $k = (1, 2, \cdots, q+3)$, is the kth element of the coefficient set $\mathcal{D}^{[q]}_{2vx}$, and the notation $R^{[q]}_{2vx}$ is used to denote the terms in square brackets.

$$\begin{aligned}\frac{\partial^2 v_5}{\partial y^2} &= \mathcal{D}^{[q]}_{2vy}(1)v_4 + \mathcal{D}^{[q]}_{2vy}(2)v_5 + \mathcal{D}^{[q]}_{2vy}(3)v_6 + \\ &\left[\mathcal{D}^{[q]}_{2vy}(4)\frac{\partial^2 v_4}{\partial y^2} + \mathcal{D}^{[q]}_{2vy}(5)\frac{\partial^2 v_6}{\partial y^2} + \cdots + \mathcal{D}^{[q]}_{2vy}(q+2)\frac{\partial^{q/2+1} v_4}{\partial y^{q/2+1}} + \mathcal{D}^{[q]}_{2vy}(q+3)\frac{\partial^{q/2+1} v_6}{\partial y^{q/2+1}}\right], \\ &= \mathcal{D}^{[q]}_{2vy}(1)v_4 + \mathcal{D}^{[q]}_{2vy}(2)v_5 + \mathcal{D}^{[q]}_{2vy}(3)v_6 + R^{[q]}_{2vy}, \end{aligned} \tag{20}$$

where $\mathcal{D}^{[q]}_{2vy}(k)$, $k = (1, 2, \cdots, q+3)$, is the kth element of the coefficient set $\mathcal{D}^{[q]}_{2vy}$, and the notation $R^{[q]}_{2vy}$ is used to denote the terms in square brackets.

Equation (18) thus reduces to

$$\left(\mathcal{D}^{[q]}_{2vx}(1)v_2 + \mathcal{D}^{[q]}_{2vx}(2)v_5 + \mathcal{D}^{[q]}_{2vx}(3)v_8\right) + \left(\mathcal{D}^{[q]}_{2vy}(1)v_4 + \mathcal{D}^{[q]}_{2vy}(2)v_5 + \mathcal{D}^{[q]}_{2vy}(3)v_6\right) = b_5 - R^{[q]}_{2vx} - R^{[q]}_{2vy}. \tag{21}$$

A next step is to express the nodal values of v on the left side of (21) in terms of the nodal values of u. Through equation (3) and by means of an IRBF scheme of order q, the following expressions are obtained.

At the central node $\mathbf{x}_5$,

$$v_5 = \frac{\partial^2 u_5}{\partial x^2} + \frac{\partial^2 u_5}{\partial y^2}, \tag{22}$$

where

$$\begin{aligned}\frac{\partial^2 u_5}{\partial x^2} &= \mathcal{D}^{[q]}_{2ux}(1)u_2 + \mathcal{D}^{[q]}_{2ux}(2)u_5 + \mathcal{D}^{[q]}_{2ux}(3)u_8 + \\ &\left[\mathcal{D}^{[q]}_{2ux}(4)\frac{\partial u_2}{\partial x} + \mathcal{D}^{[q]}_{2ux}(5)\frac{\partial u_8}{\partial x} + \cdots + \mathcal{D}^{[q]}_{2ux}(q+2)\frac{\partial^{q/2} u_2}{\partial x^{q/2}} + \mathcal{D}^{[q]}_{2ux}(q+3)\frac{\partial^{q/2} u_8}{\partial x^{q/2}}\right], \\ &= \mathcal{D}^{[q]}_{2ux}(1)u_4 + \mathcal{D}^{[q]}_{2ux}(2)u_5 + \mathcal{D}^{[q]}_{2ux}(3)u_6 + R^{[q]}_{2ux}, \end{aligned} \tag{23}$$

and

$$\begin{aligned}\frac{\partial^2 u_5}{\partial y^2} &= \mathcal{D}^{[q]}_{2uy}(1)u_4 + \mathcal{D}^{[q]}_{2uy}(2)u_5 + \mathcal{D}^{[q]}_{2uy}(3)u_6 + \\ &\left[\mathcal{D}^{[q]}_{2uy}(4)\frac{\partial u_4}{\partial y} + \mathcal{D}^{[q]}_{2uy}(5)\frac{\partial u_6}{\partial y} + \cdots + \mathcal{D}^{[q]}_{2uy}(q+2)\frac{\partial^{q/2} u_4}{\partial y^{q/2}} + \mathcal{D}^{[q]}_{2uy}(q+3)\frac{\partial^{q/2} u_6}{\partial y^{q/2}}\right], \\ &= \mathcal{D}^{[q]}_{2uy}(1)u_2 + \mathcal{D}^{[q]}_{2uy}(2)u_5 + \mathcal{D}^{[q]}_{2uy}(3)u_8 + R^{[q]}_{2uy}. \end{aligned} \tag{24}$$

At the left node $\mathbf{x}_2$,

$$v_2 = \frac{\partial^2 u_2}{\partial x^2} + \frac{\partial^2 u_2}{\partial y^2}, \tag{25}$$

$$= \mathcal{D}^{[q]}_{2uy}(1)u_1 + \mathcal{D}^{[q]}_{2uy}(2)u_2 + \mathcal{D}^{[q]}_{2uy}(3)u_3 + R^{[q]}_{2uL}, \tag{26}$$

where

$$R^{[q]}_{2uL} = \frac{\partial^2 u_2}{\partial x^2} + \left[\mathcal{D}^{[q]}_{2uy}(4)\frac{\partial u_1}{\partial y} + \mathcal{D}^{[q]}_{2uy}(5)\frac{\partial u_3}{\partial y} + \cdots + \mathcal{D}^{[q]}_{2uy}(q+2)\frac{\partial^{q/2} u_1}{\partial y^{q/2}} + \mathcal{D}^{[q]}_{2uy}(q+3)\frac{\partial^{q/2} u_3}{\partial y^{q/2}}\right]. \tag{27}$$

At the right node $\mathbf{x}_8$,

$$v_8 = \frac{\partial^2 u_8}{\partial x^2} + \frac{\partial^2 u_8}{\partial y^2}, \tag{28}$$

$$= \mathcal{D}^{[q]}_{2uy}(1)u_7 + \mathcal{D}^{[q]}_{2uy}(2)u_8 + \mathcal{D}^{[q]}_{2uy}(3)u_9 + R^{[q]}_{2uR}, \tag{29}$$

where

$$R_{2uR}^{[q]} = \frac{\partial^2 u_8}{\partial x^2} + \left[\mathcal{D}_{2uy}^{[q]}(4)\frac{\partial u_7}{\partial y} + \mathcal{D}_{2uy}^{[q]}(5)\frac{\partial u_9}{\partial y} + \cdots + \mathcal{D}_{2uy}^{[q]}(q+2)\frac{\partial^{q/2} u_7}{\partial y^{q/2}} + \mathcal{D}_{2uy}^{[q]}(q+3)\frac{\partial^{q/2} u_9}{\partial y^{q/2}} \right]. \tag{30}$$

At the bottom node $\mathbf{x}_4$,

$$v_4 = \frac{\partial^2 u_4}{\partial x^2} + \frac{\partial^2 u_4}{\partial y^2}, \tag{31}$$

$$= \mathcal{D}_{2ux}^{[q]}(1)u_1 + \mathcal{D}_{2ux}^{[q]}(2)u_4 + \mathcal{D}_{2ux}^{[q]}(3)u_7 + R_{2uB}^{[q]}, \tag{32}$$

where

$$R_{2uB}^{[q]} = \frac{\partial^2 u_4}{\partial y^2} + \left[\mathcal{D}_{2ux}^{[q]}(4)\frac{\partial u_1}{\partial x} + \mathcal{D}_{2ux}^{[q]}(5)\frac{\partial u_7}{\partial x} + \cdots + \mathcal{D}_{2ux}^{[q]}(q+2)\frac{\partial^{q/2} u_1}{\partial x^{q/2}} + \mathcal{D}_{2uy}^{[q]}(q+3)\frac{\partial^{q/2} u_7}{\partial x^{q/2}} \right]. \tag{33}$$

At the top node $\mathbf{x}_6$,

$$v_6 = \frac{\partial^2 u_6}{\partial x^2} + \frac{\partial^2 u_6}{\partial y^2}, \tag{34}$$

$$= \mathcal{D}_{2ux}^{[q]}(1)u_3 + \mathcal{D}_{2ux}^{[q]}(2)u_6 + \mathcal{D}_{2ux}^{[q]}(3)u_9 + R_{2uT}^{[q]}, \tag{35}$$

where

$$R_{2uT}^{[q]} = \frac{\partial^2 u_6}{\partial y^2} + \left[\mathcal{D}_{2ux}^{[q]}(4)\frac{\partial u_3}{\partial x} + \mathcal{D}_{2ux}^{[q]}(5)\frac{\partial u_9}{\partial x} + \cdots + \mathcal{D}_{2ux}^{[q]}(q+2)\frac{\partial^{q/2} u_3}{\partial x^{q/2}} + \mathcal{D}_{2uy}^{[q]}(q+3)\frac{\partial^{q/2} u_9}{\partial x^{q/2}} \right]. \tag{36}$$

The proposed IRBF discretisation thus results in an algebraic equation that can be described in the following form

$$F_1(u_1, u_2, \cdots, u_9) = b_5 + F_2(\frac{\partial u_i}{\partial x}, \frac{\partial u_i}{\partial y}, \cdots, \frac{\partial^2 v_j}{\partial x^2}, \frac{\partial^2 v_j}{\partial y^2}, \cdots), \tag{37}$$

where F_1 is a function of u at the nine grid points of the stencil and F_2 is a function of derivatives of u at the neighbouring nodes of the central node. An IRBF scheme of higher

order involves more derivative terms in function F_2.

3.3 Solution procedure

The nodal derivative values in function F_2 on the right side of (37) are unknown, except for the boundary values of the first derivative of u. We employ an iterative scheme to find those unknown derivative values. The solution procedure is described below:

1. Set unknown values of u and v to zero.
2. Compute the nodal values of derivatives of u along the grid lines, where the boundary values of the first derivatives of u are substituted with prescribed values.
3. Compute the nodal values of v.
4. Compute the nodal values of derivatives of v along the grid lines.
5. Solve the algebraic equation set derived from (37) for the interior nodal values of u, where the boundary values of u are substituted with prescribed values.
6. Compute CM (i.e., Convergence Measure) defined as the 2-norm ratio of the two vectors $(\mathrm{sol}^k - \mathrm{sol}^{k-1})$ and sol^k, where subscript k denotes a current iteration and sol is composed of the interior nodal values of u.
7. Check CM. If $CM < 10^{-10}$, stop the iteration and output the result. Otherwise, relax the solution, which is described in detail below, and repeat from Step 2

$$\mathrm{sol}^k = \zeta \mathrm{sol}^k + (1-\zeta)\mathrm{sol}^{k-1}, \tag{38}$$

where ζ a relax factor $(0 < \zeta \leq 1)$.

To compute the derivatives along the grid lines in Steps 2-4, we employ a global one-dimensional IRBF approximation scheme. Along a grid line, the scheme is based on

$$\frac{\partial^q f(\eta)}{\partial \eta^q} = \sum_{i=1}^{N_\eta} w_i G_i(\eta) = \sum_{i=1}^{N_\eta} w_i I_i^{(q)}(\eta), \tag{39}$$

$$\frac{\partial^{q-1} f(\eta)}{\partial \eta^{q-1}} = \sum_{i=1}^{N_\eta} w_i I_i^{(q-1)}(\eta) + c_1, \tag{40}$$

$$\cdots \quad \cdots \quad \cdots$$

$$\frac{\partial f(\eta)}{\partial \eta} = \sum_{i=1}^{N_\eta} w_i I_i^{(1)}(\eta) + c_1 \frac{\eta^{q-2}}{(q-2)!} + c_2 \frac{\eta^{q-3}}{(q-3)!} + \cdots + c_{q-1}, \tag{41}$$

$$f(\eta) = \sum_{i=1}^{N_\eta} w_i I_i^{(0)}(\eta) + c_1 \frac{\eta^{q-1}}{(q-1)!} + c_2 \frac{\eta^{q-2}}{(q-2)!} + \cdots + c_{q-1}\eta + c_q, \tag{42}$$

where N_η is the number of nodes on the grid line. To replace the IRBF coefficients and integration constants in (39)-(42) with the nodal values of f, equation (42) is enforced at η_i, $i = (1, 2, \cdots, N_\eta)$, resulting in

$$\widehat{f} = \mathcal{C}\widehat{w}, \tag{43}$$

where

$$\mathcal{C} = \begin{bmatrix} I_1^{(0)}(\eta_1), & I_2^{(0)}(\eta_1), & \cdots, & I_{N_\eta}^{(0)}(\eta_1), & \frac{\eta_1^{q-1}}{(q-1)!}, & \cdots, & \eta_1, & 1 \\ I_1^{(0)}(\eta_2), & I_2^{(0)}(\eta_2), & \cdots, & I_{N_\eta}^{(0)}(\eta_2), & \frac{\eta_2^{q-1}}{(q-1)!}, & \cdots, & \eta_2, & 1 \\ & \cdots & & \cdots & & \cdots & & \\ I_1^{(0)}(\eta_{N_\eta}), & I_2^{(0)}(\eta_{N_\eta}), & \cdots, & I_{N_\eta}^{(0)}(\eta_{N_\eta}), & \frac{\eta_{N_\eta}^{q-1}}{(q-1)!}, & \cdots, & \eta_{N_\eta}, & 1 \end{bmatrix},$$

$$\widehat{f} = \left(f_1, f_2, \cdots, f_{N_\eta}\right)^T,$$

$$\widehat{w} = \left(w_1, w_2, \cdots, w_{N_\eta}, c_1, c_2, \cdots, c_q\right)^T.$$

The minimum-norm solution to (43) is then substituted into (39)-(42).

Thus, the derivatives of f at η_j are computed using the nodal values of f

$$\frac{\partial f_j}{\partial \eta} = \left[I_1^{(1)}(\eta_j), \cdots, I_{N_\eta}^{(1)}(\eta_j), \frac{\eta^{q-2}}{(q-2)!}, \cdots, 1, 0 \right] \mathcal{C}^{-1} \widehat{f}, \quad j = (1, 2, \cdots, N_\eta), \tag{44}$$

$$\cdots \quad \cdots \quad \cdots \quad \cdots \quad \cdots \quad \cdots$$

$$\frac{\partial^q f_j}{\partial \eta^q} = \left[I_1^{(q)}(\eta_j), \cdots, I_{N_\eta}^{(q)}(\eta_j), 0, \cdots, 0, 0 \right] \mathcal{C}^{-1} \widehat{f}, \quad j = (1, 2, \cdots, N_\eta), \tag{45}$$

or

$$\widehat{\frac{\partial f}{\partial \eta}} = \mathcal{D}_1^{[q]} \widehat{f}, \tag{46}$$

$$\cdots \quad \cdots \quad \cdots$$

$$\widehat{\frac{\partial^q f}{\partial \eta^q}} = \mathcal{D}_q^{[q]} \widehat{f}, \tag{47}$$

where

$$\widehat{\frac{\partial^k f}{\partial \eta^k}} = \left(\frac{\partial^k f_1}{\partial \eta^k}, \frac{\partial^k f_2}{\partial \eta^k}, \cdots, \frac{\partial^k f_{N_\eta}}{\partial \eta^k} \right)^T, \quad k = (1, 2, \cdots, q),$$

and $\mathcal{D}_k^{[q]}$ is the differentiation matrix for computing the kth-order derivative of f. For a square region, one needs to compute the differentiation matrices on only one grid line and then can use them for the other grid lines.

It is noted that by taking appropriate derivatives as the original functions, the calculation of high-order derivatives can be based on the differentiation matrices for the first and second derivatives only. For example, in computing the third and fourth derivatives, one can consider the second derivatives as the original functions. In computing the fifth and sixth derivatives, one can consider the fourth derivatives as the original functions. With the presence of the integration constants in (39)-(42), extra information can also be included in the IRBF approximations to enhance the solution accuracy. Examples of extra information include the boundary values of the first derivative and the periodic conditions (if existed).

3.4 Implementation notes

The proposed stencil results in a sparse system matrix, which has only nine non-zero entries per row. These algebraic systems can be solved in an efficient way. On the other hand, the proposed method involves an iterative scheme for finding derivative values at the neighbouring nodes of the central node. In addition, to achieve a high level of accuracy, the method needs to use extended precision arithmetic for solving some local conversion systems in the IRBF formulation. It is noted that as shown in [25], utilisation of extended-precision floating point arithmetic is an effective way to bypass the solution of the ill-conditioned linear system. In this study, the local conversion systems are solved with 32 digits of precision, and the computation of other tasks such as computing derivatives, and forming and solving the final system of algebraic equations are all carried out with standard double precision. For the region discretised with a uniform grid, one needs to solve the conversion systems on only one stencil, and the obtained results are then used for other stencils and for every iteration step. They can be taken as a preprocessing step. Also, the final system matrix stays the same during the iteration process. The calculation of derivatives along the grid lines is simply the process of doing function approximations. Its computational efficiency can be improved by employing overlapping domain decomposition as discussed in [22].

3.5 Extensions to non-rectangular regions

The proposed stencil can be extended to solve the biharmonic equation defined on a non-rectangular region. The reason for this is that the proposed stencil involves only nodal derivative values rather than nodal PDE values. The calculation of nodal derivative values is carried out along the grid lines. Special attention is needed to compute the boundary values of v

$$v_b = \frac{\partial^2 u_b}{\partial x^2} + \frac{\partial^2 u_b}{\partial y^2}, \tag{48}$$

where the subscript b is used to denote the boundary point.

The directional derivative of function $f(x, y)$ along a curved line is given by

$$\nabla_{\mathbf{t}} f(x, y) = \mathbf{t} \cdot \nabla f(x, y) = \frac{\partial f}{\partial x} t_x + \frac{\partial f}{\partial y} t_y, \tag{49}$$

where $\mathbf{t}$ is a unit tangent vector.

Taking $f = \partial u_b / \partial x$ yields

$$\nabla_{\mathbf{t}} \left(\frac{\partial u_b}{\partial x} \right) = \frac{\partial^2 u_b}{\partial x^2} t_x + \frac{\partial^2 u_b}{\partial x \partial y} t_y, \tag{50}$$

or

$$\frac{\partial^2 u_b}{\partial x \partial y} = \frac{1}{t_y} \left(\nabla_{\mathbf{t}} \left(\frac{\partial u_b}{\partial x} \right) - \frac{\partial^2 u_b}{\partial x^2} t_x \right). \tag{51}$$

Taking $f = \partial u_b / \partial y$ yields

$$\nabla_{\mathbf{t}} \left(\frac{\partial u_b}{\partial y} \right) = \frac{\partial^2 u_b}{\partial x \partial y} t_x + \frac{\partial^2 u_b}{\partial y^2} t_y, \tag{52}$$

or

$$\frac{\partial^2 u_b}{\partial x \partial y} = \frac{1}{t_x} \left(\nabla_{\mathbf{t}} \left(\frac{\partial u_b}{\partial y} \right) - \frac{\partial^2 u_b}{\partial y^2} t_y \right). \tag{53}$$

From (51) and (53), one can derive the relationship between $\partial^2 u / \partial x^2$ and $\partial^2 u / \partial y^2$ at a boundary point

$$\frac{1}{t_y} \left(\nabla_{\mathbf{t}} \left(\frac{\partial u_b}{\partial x} \right) - \frac{\partial^2 u_b}{\partial x^2} t_x \right) = \frac{1}{t_x} \left(\nabla_{\mathbf{t}} \left(\frac{\partial u_b}{\partial y} \right) - \frac{\partial^2 u_b}{\partial y^2} t_y \right). \tag{54}$$

For boundary points on the x-grid lines, equation (48) thus reduces to the equation containing only the second derivative with respect to x

$$v_b = \left[1 + \left(\frac{t_x}{t_y} \right)^2 \right] \frac{\partial^2 u_b}{\partial x^2} + p_y, \tag{55}$$

where p_y is a known quantity

$$p_y = \frac{1}{t_y}\nabla_{\mathbf{t}}\left(\frac{\partial u_b}{\partial y}\right) - \frac{t_x}{t_y^2}\nabla_{\mathbf{t}}\left(\frac{\partial u_b}{\partial x}\right).$$

For boundary points on the y-grid lines, equation (48) thus reduces to the equation containing only the second derivative with respect to y

$$v_b = \left[1 + \left(\frac{t_y}{t_x}\right)^2\right]\frac{\partial^2 u_b}{\partial y^2} + p_x, \tag{56}$$

where p_x is a known quantity

$$p_x = \frac{1}{t_x}\nabla_{\mathbf{t}}\left(\frac{\partial u_b}{\partial x}\right) - \frac{t_y}{t_x^2}\nabla_{\mathbf{t}}\left(\frac{\partial u_b}{\partial y}\right).$$

It is noted that there is no approximation error in equations (55) and (56) [26]. For better accuracy, the boundary values $\partial u_b/\partial x$ and $\partial u_b/\partial y$ are included in the approximation of $\partial^2 u_b/\partial x^2$ in (55) and $\partial^2 u_b/\partial y^2$ in (56), respectively. It is expected that the ability of RBFs to work well with irregular nodes and the inclusion of nodal derivative values into the approximations will alleviate the loss of accuracy caused by the non-rectangular shapes of the stencil.

4 Numerical examples

4.1 Example 1

We consider the biharmonic problem defined in $-1 \leq x, y \leq 1$ with the exact solution

$$u(x, y) = \frac{1}{\pi^4}\sin(\pi x)\sin(\pi y),$$

from which the forcing term $b(x, y)$ and boundary conditions $g_1(x, y)$ and $g_2(x, y)$ are derived.

Approximations over the stencil and grid lines are carried out by using IRBFq. Four values of q, i.e. (2, 4, 6, 8), are considered.

First we study the effect of the RBF width associated with the approximations on the nine-point stencil on the solution accuracy. A wide range of the RBF width from 10^{-4} to 10^{0} is considered. The RBF width associated with the approximations on the grid lines is kept at a value of 0.001. The obtained results are displayed in Figure 2. It can be seen that the IRBF solution becomes more accurate and less dependent on the RBF width with an increase in the order of the IRBF scheme. For IRBF6 and IRBF8, the IRBF solutions are highly accurate and not influenced by the RBF width.

The proposed discretisation process involves four matrices, the conversion matrix used in solving equation (3), denoted by $\mathcal{C}_u$, the conversion matrix used in solving equation (4), denoted by $\mathcal{C}_v$, the conversion matrix in approximating the variables u and v along the grid lines, denoted by $\mathcal{C}$, and the system matrix, denoted by $\mathcal{A}$. Figure 3 shows the effect of the RBF width associated with the nine-point stencil on the condition numbers of these matrices. The four IRBF schemes produce similar values for the condition number of $\mathcal{A}$. They are quite low (i.e. $O(10^2)$), which suggests that the resultant global systems, which are large, can be handled with standard/double precision. On the other hand, an IRBF scheme of higher order produces larger values for the condition numbers of $\mathcal{C}_u$, $\mathcal{C}_v$ and $\mathcal{C}$. For IRBF6 and IRBF8 here, a higher level of precision (e.g. 32-digit accuracy) is needed. It is noted that $\mathcal{C}_u$, $\mathcal{C}_v$ and $\mathcal{C}$ are relatively-small matrices. The calculation of derivatives along the grid lines is simply the process of doing function approximations and one can utilise overlapping domain decomposition to improve its matrix condition number and efficiency.

Figure 4 shows the effect of the RBF width associated with the grid lines on the solution accuracy. A wide range of the RBF width from 10^{-4} to 10^{-1} is considered. At the smallest value of 10^{-4}, the IRBF solution converges as $O(h^{3.89})$ for IRBF4, $O(h^{6.04})$ for IRBF6 and $O(h^{8.25})$ for IRBF8. At the largest value of 10^{-1}, the IRBF solution converges as $O(h^{4.85})$ for IRBF4, $O(h^{6.85})$ for IRBF6 and $O(h^{9.59})$ for IRBF8. It can be seen that the RBF width (grid lines) also does not have a strong influence on the solution accuracy.

The CPU times used by our Matlab code for solving this problem are relatively small. For example, for a grid 21×21 and on a Laptop with an CPU Intel(R) Core(TM) i7-10610U 1.80GHz 2.30GHz, the CPU time is 0.012 seconds for solving the conversion systems on the stencil , 0.37 seconds for solving the conversion system on the grid line, and 0.0014 seconds for solving the final system matrix.

The obtained numerical results indicate that IRBF4, IRBF6 and IRBF8 using the 9 grid points are high-order approximation schemes. An IRBF scheme of higher order yields a faster convergence rate but produces a larger matrix condition number. In general, there is a need for using extended precision to handle small local systems. It should be pointed out that an IRBF scheme of high order (i.e. ≥ 6) produce solutions that are not much influenced by the RBF width.

4.2 Example 2

Unlike Example 1, the forcing function in this example is chosen as a polynomial

$$b = 8\left[3y^2(1-y)^2 + 3x^2(1-x)^2 + (6x^2-6x+1)(6y^2-6y+1)\right], \tag{57}$$

where $0 \leq x, y \leq 1$. The exact solution to this problem is

$$u = \left[(x-x^2)(y-y^2)\right]^2, \tag{58}$$

from which the boundary values of the first derivative are derived. This problem was studied by Gupta and Manohar [8], Stepheson [9] and other authors. It serves as a basis for comparison purposes. The obtained results using IRBF8 are shown in Figure 5 and Table 1. From Figure 5, like Example 1, the IRBF solutions are seen not to be influenced by the RBF widths. The numerical errors are consistently reduced with a small decrease in the grid size. In Table 1, for a given grid size, the obtained results are much more accurate than those by the conventional 13-point stencil [8] and the compact 9-point stencil [9].

4.3 Example 3

The domain of interest is chosen as a region inside the unit square and outside the circle of radius 0.125 as shown in Figure 6. The square and circle are both centered at the origin. The forcing function and exact solution are given by

$$b = (2\pi)^4 \left[4\cos(2\pi x)\cos(2\pi y) - \cos(2\pi x) - \cos(2\pi y)\right], \tag{59}$$

$$u = \left[1 - \cos(2\pi x)\right]\left[1 - \cos(2\pi y)\right]. \tag{60}$$

The boundary values of the first derivative are derived from (60). We also use a Cartesian grid to represent the domain. Let h be the grid size. Grid nodes close to the inner boundary (within distance $h/6$) and those inside the circle are removed. Boundary nodes are intersections of the grid lines and the boundaries. When the density is increased, the grid becomes more non-uniform. With the presence of inner boundary nodes, the minimum distance between nodes becomes smaller. In this regard, a range of the RBF width is chosen as $[10^{-5}, 10^{-2}]$ instead of $[10^{-4}, 10^{-1}]$. The obtained results using IRBF6 are shown in Figure 7. It can be seen that similar levels of the solution accuracy are obtained. The solution converges fast with grid refinement for any value of the RBF width. For example, taking the RBF width of 0.001 for the approximation on the stencils and 0.01 for the approximation on the grid lines, the rate of convergence is 9.03.

5 Concluding remarks

This paper reports a new compact 9-point stencil based on IRBFs for solving the first biharmonic problem in two dimensions. Using integration to construct the RBF approximations has its own strengths. Through integration, nodal derivative values are included in the 9-point stencil in a natural way. The higher the order of an IRBF scheme used, the greater the number of the derivative terms is included. It is found that employing a high-order IRBF scheme on the stencil results in a solution that is highly accurate and not influenced by the

RBF width. With extra information being derivatives along the grid lines, the proposed compact stencil can also be used for problems with curved boundaries. In numerical examples, the proposed stencil compares favourably with the conventional 13-point and 9-point stencils, and high-order convergence of the proposed IRBF process is achieved for problems defined on rectangular and non-rectangular domains.

Appendix

Analytical forms: The following are integrated basis functions derived from the multiquadric function by using Mathematica

$$
\begin{aligned}
I_i^{(1)}(\eta) &= \tfrac{(\eta-\eta_i)}{2}A + \tfrac{a_i^2}{2}B,\\
I_i^{(2)}(\eta) &= \left(\tfrac{-a_i^2}{3} + \tfrac{(\eta-\eta_i)^2}{6}\right)A + \tfrac{a_i^2(\eta-\eta_i)}{2}B,\\
I_i^{(3)}(\eta) &= \left(\tfrac{-13a_i^2(\eta-\eta_i)}{48} + \tfrac{(\eta-\eta_i)^3}{24}\right)A + \left(\tfrac{-a_i^4}{16} + \tfrac{a_i^2(\eta-\eta_i)^2}{4}\right)B,\\
I_i^{(4)}(\eta) &= \left(\tfrac{a_i^4}{45} - \tfrac{83a_i^2(\eta-\eta_i)^2}{720} + \tfrac{(\eta-\eta_i)^4}{120}\right)A + \left(\tfrac{-3a_i^4(\eta-\eta_i)}{48} + \tfrac{4a_i^2(\eta-\eta_i)^3}{48}\right)B,\\
I_i^{(5)}(\eta) &= \left(\tfrac{113a_i^4(\eta-\eta_i)}{5760} - \tfrac{97a_i^2(\eta-\eta_i)^3}{2880} + \tfrac{(\eta-\eta_i)^5}{720}\right)A + \left(\tfrac{a_i^6}{384} - \tfrac{3a_i^4(\eta-\eta_i)^2}{96} + \tfrac{2a_i^2(\eta-\eta_i)^4}{96}\right)B,\\
I_i^{(6)}(\eta) &= \left(\tfrac{-a_i^6}{1575} + \tfrac{593a_i^4(\eta-\eta_i)^2}{67200} - \tfrac{253a_i^2(\eta-\eta_i)^4}{33600} + \tfrac{(\eta-\eta_i)^6}{5040}\right)A+\\
&\quad \left(\tfrac{5a_i^6(\eta-\eta_i)}{1920} - \tfrac{20a_i^4(\eta-\eta_i)^3}{1920} + \tfrac{8a_i^2(\eta-\eta_i)^5}{1920}\right)B,\\
I_i^{(7)}(\eta) &= \left(\tfrac{-1873a_i^6(\eta-\eta_i)}{3225600} + \tfrac{4327a_i^4(\eta-\eta_i)^3}{1612800} - \tfrac{551a_i^2(\eta-\eta_i)^5}{403200} + \tfrac{(\eta-\eta_i)^7}{403200}\right)A+\\
&\quad \left(\tfrac{-a_i^8}{18432} + \tfrac{15a_i^6(\eta-\eta_i)^2}{11520} - \tfrac{30a_i^4(\eta-\eta_i)^4}{11520} + \tfrac{8a_i^2(\eta-\eta_i)^6}{11520}\right)B,\\
I_i^{(8)}(\eta) &= \left(\tfrac{a_i^8}{99225} - \tfrac{54511a_i^6(\eta-\eta_i)^2}{203212800} + \tfrac{20939a_i^4(\eta-\eta_i)^4}{33868800} - \tfrac{5309a_i^2(\eta-\eta_i)^6}{25401600} + \tfrac{(\eta-\eta_i)^8}{362880}\right)A+\\
&\quad \left(\tfrac{-35a_i^8(\eta-\eta_i)}{645120} + \tfrac{280a_i^6(\eta-\eta_i)^3}{645120} - \tfrac{336a_i^4(\eta-\eta_i)^5}{645120} + \tfrac{64a_i^2(\eta-\eta_i)^7}{645120}\right)B,
\end{aligned}
$$

where $A = \sqrt{(\eta-\eta_i)^2 + a_i^2}$ and $B = \ln\left((\eta-\eta_i) + \sqrt{(\eta-\eta_i)^2 + a_i^2}\right)$.

Conversion systems: The following are the systems used for the conversion of the RBF space into the physical space for the variables u and v.

IRBF2:

$$\begin{pmatrix} u_{i-1} \\ u_i \\ u_{i+1} \\ \frac{\partial u_{i-1}}{\partial \eta} \\ \frac{\partial u_{i+1}}{\partial \eta} \end{pmatrix} = \begin{bmatrix} I_1^{(0)}(\eta_{i-1}) & I_3^{(0)}(\eta_{i-1}) & I_3^{(0)}(\eta_{i-1}) & \eta_{i-1} & 1 \\ I_1^{(0)}(\eta_i) & I_3^{(0)}(\eta_i) & I_3^{(0)}(\eta_i) & \eta_i & 1 \\ I_1^{(0)}(\eta_{i+1}) & I_3^{(0)}(\eta_{i+1}) & I_3^{(0)}(\eta_{i+1}) & \eta_{i+1} & 1 \\ I_1^{(1)}(\eta_{i-1}) & I_3^{(1)}(\eta_{i-1}) & I_3^{(1)}(\eta_{i-1}) & 1 & 0 \\ I_1^{(1)}(\eta_{i+1}) & I_3^{(1)}(\eta_{i+1}) & I_3^{(1)}(\eta_{i+1}) & 1 & 0 \end{bmatrix} \begin{pmatrix} w_1 \\ w_2 \\ w_3 \\ c_1 \\ c_2 \end{pmatrix}, \tag{61}$$

$$\begin{pmatrix} v_{i-1} \\ v_i \\ v_{i+1} \\ \frac{\partial^2 v_{i-1}}{\partial \eta^2} \\ \frac{\partial^2 v_{i+1}}{\partial \eta^2} \end{pmatrix} = \begin{bmatrix} I_1^{(0)}(\eta_{i-1}) & I_3^{(0)}(\eta_{i-1}) & I_3^{(0)}(\eta_{i-1}) & \eta_{i-1} & 1 \\ I_1^{(0)}(\eta_i) & I_3^{(0)}(\eta_i) & I_3^{(0)}(\eta_i) & \eta_i & 1 \\ I_1^{(0)}(\eta_{i+1}) & I_3^{(0)}(\eta_{i+1}) & I_3^{(0)}(\eta_{i+1}) & \eta_{i+1} & 1 \\ I_1^{(2)}(\eta_{i-1}) & I_3^{(2)}(\eta_{i-1}) & I_3^{(2)}(\eta_{i-1}) & 0 & 0 \\ I_1^{(2)}(\eta_{i+1}) & I_3^{(2)}(\eta_{i+1}) & I_3^{(2)}(\eta_{i+1}) & 0 & 0 \end{bmatrix} \begin{pmatrix} w_1 \\ w_2 \\ w_3 \\ c_1 \\ c_2 \end{pmatrix}, \tag{62}$$

IRBF4:

$$\begin{pmatrix} u_{i-1} \\ u_i \\ u_{i+1} \\ \frac{\partial u_{i-1}}{\partial \eta} \\ \frac{\partial u_{i+1}}{\partial \eta} \\ \frac{\partial^2 u_{i-1}}{\partial \eta^2} \\ \frac{\partial^2 u_{i+1}}{\partial \eta^2} \end{pmatrix} = \begin{bmatrix} I_1^{(0)}(\eta_{i-1}) & I_3^{(0)}(\eta_{i-1}) & I_3^{(0)}(\eta_{i-1}) & \frac{\eta_{i-1}^3}{3!} & \frac{\eta_{i-1}^2}{2} & \eta_{i-1} & 1 \\ I_1^{(0)}(\eta_i) & I_3^{(0)}(\eta_i) & I_3^{(0)}(\eta_i) & \frac{\eta_i^3}{3!} & \frac{\eta_i^2}{2} & \eta_i & 1 \\ I_1^{(0)}(\eta_{i+1}) & I_3^{(0)}(\eta_{i+1}) & I_3^{(0)}(\eta_{i+1}) & \frac{\eta_{i+1}^3}{3!} & \frac{\eta_{i+1}^2}{2} & \eta_{i+1} & 1 \\ I_1^{(1)}(\eta_{i-1}) & I_3^{(1)}(\eta_{i-1}) & I_3^{(1)}(\eta_{i-1}) & \frac{\eta_{i-1}^2}{2} & \eta_{i-1} & 1 & 0 \\ I_1^{(1)}(\eta_{i+1}) & I_3^{(1)}(\eta_{i+1}) & I_3^{(1)}(\eta_{i+1}) & \frac{\eta_{i+1}^2}{2} & \eta_{i+1} & 1 & 0 \\ I_1^{(2)}(\eta_{i-1}) & I_3^{(2)}(\eta_{i-1}) & I_3^{(2)}(\eta_{i-1}) & \eta_{i-1} & 1 & 0 & 0 \\ I_1^{(2)}(\eta_{i+1}) & I_3^{(2)}(\eta_{i+1}) & I_3^{(2)}(\eta_{i+1}) & \eta_{i+1} & 1 & 0 & 0 \end{bmatrix} \begin{pmatrix} w_1 \\ w_2 \\ w_3 \\ c_1 \\ c_2 \\ c_3 \\ c_4 \end{pmatrix}, \tag{63}$$

$$\begin{pmatrix} v_{i-1} \\ v_i \\ v_{i+1} \\ \frac{\partial^2 v_{i-1}}{\partial \eta^2} \\ \frac{\partial^2 v_{i+1}}{\partial \eta^2} \\ \frac{\partial^3 v_{i-1}}{\partial \eta^3} \\ \frac{\partial^3 v_{i+1}}{\partial \eta^3} \end{pmatrix} = \begin{bmatrix} I_1^{(0)}(\eta_{i-1}) & I_3^{(0)}(\eta_{i-1}) & I_3^{(0)}(\eta_{i-1}) & \frac{\eta_{i-1}^3}{3!} & \frac{\eta_{i-1}^2}{2} & \eta_{i-1} & 1 \\ I_1^{(0)}(\eta_i) & I_3^{(0)}(\eta_i) & I_3^{(0)}(\eta_i) & \frac{\eta_i^3}{3!} & \frac{\eta_i^2}{2} & \eta_i & 1 \\ I_1^{(0)}(\eta_{i+1}) & I_3^{(0)}(\eta_{i+1}) & I_3^{(0)}(\eta_{i+1}) & \frac{\eta_{i+1}^3}{3!} & \frac{\eta_{i+1}^2}{2} & \eta_{i+1} & 1 \\ I_1^{(2)}(\eta_{i-1}) & I_3^{(2)}(\eta_{i-1}) & I_3^{(2)}(\eta_{i-1}) & \eta_{i-1} & 1 & 0 & 0 \\ I_1^{(2)}(\eta_{i+1}) & I_3^{(2)}(\eta_{i+1}) & I_3^{(2)}(\eta_{i+1}) & \eta_{i+1} & 1 & 0 & 0 \\ I_1^{(3)}(\eta_{i-1}) & I_3^{(3)}(\eta_{i-1}) & I_3^{(3)}(\eta_{i-1}) & 1 & 0 & 0 & 0 \\ I_1^{(3)}(\eta_{i+1}) & I_3^{(3)}(\eta_{i+1}) & I_3^{(3)}(\eta_{i+1}) & 1 & 0 & 0 & 0 \end{bmatrix} \begin{pmatrix} w_1 \\ w_2 \\ w_3 \\ c_1 \\ c_2 \\ c_3 \\ c_4 \end{pmatrix}, \tag{64}$$

IRBF6:

$$\begin{pmatrix} u_{i-1} \\ u_i \\ u_{i+1} \\ \frac{\partial u_{i-1}}{\partial \eta} \\ \frac{\partial u_{i+1}}{\partial \eta} \\ \frac{\partial^2 u_{i-1}}{\partial \eta^2} \\ \frac{\partial^2 u_{i+1}}{\partial \eta^2} \\ \frac{\partial^3 u_{i-1}}{\partial \eta^3} \\ \frac{\partial^3 u_{i+1}}{\partial \eta^3} \end{pmatrix} = \begin{bmatrix} I_1^{(0)}(\eta_{i-1}) & I_3^{(0)}(\eta_{i-1}) & I_3^{(0)}(\eta_{i-1}) & \frac{\eta_{i-1}^5}{5!} & \frac{\eta_{i-1}^4}{4!} & \cdots & \eta_{i-1} & 1 \\ I_1^{(0)}(\eta_i) & I_3^{(0)}(\eta_i) & I_3^{(0)}(\eta_i) & \frac{\eta_i^5}{5!} & \frac{\eta_i^4}{4!} & \cdots & \eta_i & 1 \\ I_1^{(0)}(\eta_{i+1}) & I_3^{(0)}(\eta_{i+1}) & I_3^{(0)}(\eta_{i+1}) & \frac{\eta_{i+1}^5}{5!} & \frac{\eta_{i+1}^4}{4!} & \cdots & \eta_{i+1} & 1 \\ I_1^{(1)}(\eta_{i-1}) & I_3^{(1)}(\eta_{i-1}) & I_3^{(1)}(\eta_{i-1}) & \frac{\eta_{i-1}^4}{4!} & \frac{\eta_{i-1}^3}{3!} & \cdots & 1 & 0 \\ I_1^{(1)}(\eta_{i+1}) & I_3^{(1)}(\eta_{i+1}) & I_3^{(1)}(\eta_{i+1}) & \frac{\eta_{i+1}^4}{4!} & \frac{\eta_{i+1}^3}{3!} & \cdots & 1 & 0 \\ I_1^{(2)}(\eta_{i-1}) & I_3^{(2)}(\eta_{i-1}) & I_3^{(2)}(\eta_{i-1}) & \frac{\eta_{i-1}^3}{3!} & \frac{\eta_{i-1}^2}{2} & \cdots & 0 & 0 \\ I_1^{(2)}(\eta_{i+1}) & I_3^{(2)}(\eta_{i+1}) & I_3^{(2)}(\eta_{i+1}) & \frac{\eta_{i+1}^3}{3!} & \frac{\eta_{i+1}^2}{2} & \cdots & 0 & 0 \\ I_1^{(3)}(\eta_{i-1}) & I_3^{(3)}(\eta_{i-1}) & I_3^{(3)}(\eta_{i-1}) & \frac{\eta_{i-1}^2}{2} & \eta_{i-1} & \cdots & 0 & 0 \\ I_1^{(3)}(\eta_{i+1}) & I_3^{(3)}(\eta_{i+1}) & I_3^{(3)}(\eta_{i+1}) & \frac{\eta_{i+1}^2}{2} & \eta_{i+1} & \cdots & 0 & 0 \end{bmatrix} \begin{pmatrix} w_1 \\ w_2 \\ w_3 \\ c_1 \\ c_2 \\ c_3 \\ c_4 \\ c_5 \\ c_6 \end{pmatrix}, \tag{65}$$

$$\begin{pmatrix} v_{i-1} \\ v_i \\ v_{i+1} \\ \frac{\partial^2 v_{i-1}}{\partial \eta^2} \\ \frac{\partial^2 v_{i+1}}{\partial \eta^2} \\ \frac{\partial^3 v_{i-1}}{\partial \eta^3} \\ \frac{\partial^3 v_{i+1}}{\partial \eta^3} \\ \frac{\partial^4 v_{i-1}}{\partial \eta^3} \\ \frac{\partial^4 v_{i+1}}{\partial \eta^3} \end{pmatrix} = \begin{bmatrix} I_1^{(0)}(\eta_{i-1}) & I_3^{(0)}(\eta_{i-1}) & I_3^{(0)}(\eta_{i-1}) & \frac{\eta_{i-1}^5}{5!} & \frac{\eta_{i-1}^4}{4!} & \cdots & \eta_{i-1} & 1 \\ I_1^{(0)}(\eta_i) & I_3^{(0)}(\eta_i) & I_3^{(0)}(\eta_i) & \frac{\eta_i^5}{5!} & \frac{\eta_i^4}{4!} & \cdots & \eta_i & 1 \\ I_1^{(0)}(\eta_{i+1}) & I_3^{(0)}(\eta_{i+1}) & I_3^{(0)}(\eta_{i+1}) & \frac{\eta_{i+1}^5}{5!} & \frac{\eta_{i+1}^4}{4!} & \cdots & \eta_{i+1} & 1 \\ I_1^{(2)}(\eta_{i-1}) & I_3^{(2)}(\eta_{i-1}) & I_3^{(2)}(\eta_{i-1}) & \frac{\eta_{i-1}^3}{3!} & \frac{\eta_{i-1}^2}{2} & \cdots & 0 & 0 \\ I_1^{(2)}(\eta_{i+1}) & I_3^{(2)}(\eta_{i+1}) & I_3^{(2)}(\eta_{i+1}) & \frac{\eta_{i+1}^3}{3!} & \frac{\eta_{i+1}^2}{2} & \cdots & 0 & 0 \\ I_1^{(3)}(\eta_{i-1}) & I_3^{(3)}(\eta_{i-1}) & I_3^{(3)}(\eta_{i-1}) & \frac{\eta_{i-1}^2}{2} & \eta_{i-1} & \cdots & 0 & 0 \\ I_1^{(3)}(\eta_{i+1}) & I_3^{(3)}(\eta_{i+1}) & I_3^{(3)}(\eta_{i+1}) & \frac{\eta_{i+1}^2}{2} & \eta_{i+1} & \cdots & 0 & 0 \\ I_1^{(4)}(\eta_{i-1}) & I_3^{(4)}(\eta_{i-1}) & I_3^{(4)}(\eta_{i-1}) & \eta_{i-1} & 1 & \cdots & 0 & 0 \\ I_1^{(4)}(\eta_{i+1}) & I_3^{(4)}(\eta_{i+1}) & I_3^{(4)}(\eta_{i+1}) & \eta_{i+1} & 1 & \cdots & 0 & 0 \end{bmatrix} \begin{pmatrix} w_1 \\ w_2 \\ w_3 \\ c_1 \\ c_2 \\ c_3 \\ c_4 \\ c_5 \\ c_6 \end{pmatrix}, \tag{66}$$

IRBF8:

$$\begin{pmatrix} u_{i-1} \\ u_i \\ u_{i+1} \\ \frac{\partial u_{i-1}}{\partial \eta} \\ \frac{\partial u_{i+1}}{\partial \eta} \\ \frac{\partial^2 u_{i-1}}{\partial \eta^2} \\ \frac{\partial^2 u_{i+1}}{\partial \eta^2} \\ \frac{\partial^3 u_{i-1}}{\partial \eta^3} \\ \frac{\partial^3 u_{i+1}}{\partial \eta^3} \\ \frac{\partial^4 u_{i-1}}{\partial \eta^4} \\ \frac{\partial^4 u_{i+1}}{\partial \eta^4} \end{pmatrix} = \begin{bmatrix} I_1^{(0)}(\eta_{i-1}) & I_3^{(0)}(\eta_{i-1}) & I_3^{(0)}(\eta_{i-1}) & \frac{\eta_{i-1}^7}{7!} & \frac{\eta_{i-1}^6}{6!} & \cdots & \eta_{i-1} & 1 \\ I_1^{(0)}(\eta_i) & I_3^{(0)}(\eta_i) & I_3^{(0)}(\eta_i) & \frac{\eta_i^7}{7!} & \frac{\eta_i^6}{6!} & \cdots & \eta_i & 1 \\ I_1^{(0)}(\eta_{i+1}) & I_3^{(0)}(\eta_{i+1}) & I_3^{(0)}(\eta_{i+1}) & \frac{\eta_{i+1}^7}{7!} & \frac{\eta_{i+1}^6}{6!} & \cdots & \eta_{i+1} & 1 \\ I_1^{(1)}(\eta_{i-1}) & I_3^{(1)}(\eta_{i-1}) & I_3^{(1)}(\eta_{i-1}) & \frac{\eta_{i-1}^6}{6!} & \frac{\eta_{i-1}^5}{5!} & \cdots & 1 & 0 \\ I_1^{(1)}(\eta_{i+1}) & I_3^{(1)}(\eta_{i+1}) & I_3^{(1)}(\eta_{i+1}) & \frac{\eta_{i+1}^6}{6!} & \frac{\eta_{i+1}^5}{5!} & \cdots & 1 & 0 \\ I_1^{(2)}(\eta_{i-1}) & I_3^{(2)}(\eta_{i-1}) & I_3^{(2)}(\eta_{i-1}) & \frac{\eta_{i-1}^5}{5!} & \frac{\eta_{i-1}^4}{4!} & \cdots & 0 & 0 \\ I_1^{(2)}(\eta_{i+1}) & I_3^{(2)}(\eta_{i+1}) & I_3^{(2)}(\eta_{i+1}) & \frac{\eta_{i+1}^5}{5!} & \frac{\eta_{i+1}^4}{4!} & \cdots & 0 & 0 \\ I_1^{(3)}(\eta_{i-1}) & I_3^{(3)}(\eta_{i-1}) & I_3^{(3)}(\eta_{i-1}) & \frac{\eta_{i-1}^4}{4!} & \frac{\eta_{i-1}^3}{3!} & \cdots & 0 & 0 \\ I_1^{(3)}(\eta_{i+1}) & I_3^{(3)}(\eta_{i+1}) & I_3^{(3)}(\eta_{i+1}) & \frac{\eta_{i+1}^4}{4!} & \frac{\eta_{i+1}^3}{3!} & \cdots & 0 & 0 \\ I_1^{(4)}(\eta_{i-1}) & I_3^{(4)}(\eta_{i-1}) & I_3^{(4)}(\eta_{i-1}) & \frac{\eta_{i-1}^3}{3!} & \frac{\eta_{i-1}^2}{2} & \cdots & 0 & 0 \\ I_1^{(4)}(\eta_{i+1}) & I_3^{(4)}(\eta_{i+1}) & I_3^{(4)}(\eta_{i+1}) & \frac{\eta_{i+1}^3}{3!} & \frac{\eta_{i+1}^2}{2} & \cdots & 0 & 0 \end{bmatrix} \begin{pmatrix} w_1 \\ w_2 \\ w_3 \\ c_1 \\ c_2 \\ c_3 \\ c_4 \\ c_5 \\ c_6 \\ c_7 \\ c_8 \end{pmatrix}, \tag{67}$$

$$\begin{pmatrix} v_{i-1} \\ v_i \\ v_{i+1} \\ \frac{\partial^2 v_{i-1}}{\partial \eta^2} \\ \frac{\partial^2 v_{i+1}}{\partial \eta^2} \\ \frac{\partial^3 v_{i-1}}{\partial \eta^3} \\ \frac{\partial^3 v_{i+1}}{\partial \eta^3} \\ \frac{\partial^4 v_{i-1}}{\partial \eta^4} \\ \frac{\partial^4 v_{i+1}}{\partial \eta^4} \\ \frac{\partial^5 v_{i-1}}{\partial \eta^5} \\ \frac{\partial^5 v_{i+1}}{\partial \eta^5} \end{pmatrix} = \begin{bmatrix} I_1^{(0)}(\eta_{i-1}) & I_3^{(0)}(\eta_{i-1}) & I_3^{(0)}(\eta_{i-1}) & \frac{\eta_{i-1}^7}{7!} & \frac{\eta_{i-1}^6}{6!} & \cdots & \eta_{i-1} & 1 \\ I_1^{(0)}(\eta_i) & I_3^{(0)}(\eta_i) & I_3^{(0)}(\eta_i) & \frac{\eta_i^7}{7!} & \frac{\eta_i^6}{6!} & \cdots & \eta_i & 1 \\ I_1^{(0)}(\eta_{i+1}) & I_3^{(0)}(\eta_{i+1}) & I_3^{(0)}(\eta_{i+1}) & \frac{\eta_{i+1}^7}{7!} & \frac{\eta_{i+1}^6}{6!} & \cdots & \eta_{i+1} & 1 \\ I_1^{(2)}(\eta_{i-1}) & I_3^{(2)}(\eta_{i-1}) & I_3^{(2)}(\eta_{i-1}) & \frac{\eta_{i-1}^5}{5!} & \frac{\eta_{i-1}^4}{4!} & \cdots & 0 & 0 \\ I_1^{(2)}(\eta_{i+1}) & I_3^{(2)}(\eta_{i+1}) & I_3^{(2)}(\eta_{i+1}) & \frac{\eta_{i+1}^5}{5!} & \frac{\eta_{i+1}^4}{4!} & \cdots & 0 & 0 \\ I_1^{(3)}(\eta_{i-1}) & I_3^{(3)}(\eta_{i-1}) & I_3^{(3)}(\eta_{i-1}) & \frac{\eta_{i-1}^4}{4!} & \frac{\eta_{i-1}^3}{3!} & \cdots & 0 & 0 \\ I_1^{(3)}(\eta_{i+1}) & I_3^{(3)}(\eta_{i+1}) & I_3^{(3)}(\eta_{i+1}) & \frac{\eta_{i+1}^4}{4!} & \frac{\eta_{i+1}^3}{3!} & \cdots & 0 & 0 \\ I_1^{(4)}(\eta_{i-1}) & I_3^{(4)}(\eta_{i-1}) & I_3^{(4)}(\eta_{i-1}) & \frac{\eta_{i-1}^3}{3!} & \frac{\eta_{i-1}^2}{2} & \cdots & 0 & 0 \\ I_1^{(4)}(\eta_{i+1}) & I_3^{(4)}(\eta_{i+1}) & I_3^{(4)}(\eta_{i+1}) & \frac{\eta_{i+1}^3}{3!} & \frac{\eta_{i+1}^2}{2} & \cdots & 0 & 0 \\ I_1^{(5)}(\eta_{i-1}) & I_3^{(5)}(\eta_{i-1}) & I_3^{(5)}(\eta_{i-1}) & \frac{\eta_{i-1}^2}{2} & \eta_{i-1} & \cdots & 0 & 0 \\ I_1^{(5)}(\eta_{i+1}) & I_3^{(5)}(\eta_{i+1}) & I_3^{(5)}(\eta_{i+1}) & \frac{\eta_{i+1}^2}{2} & \eta_{i+1} & \cdots & 0 & 0 \end{bmatrix} \begin{pmatrix} w_1 \\ w_2 \\ w_3 \\ c_1 \\ c_2 \\ c_3 \\ c_4 \\ c_5 \\ c_6 \\ c_7 \\ c_8 \end{pmatrix}, \tag{68}$$

References

1. Collatz L. The Numerical Treatment of Differential Equations. Berlin: Springer–Verlag;

1960.

2. Mai-Duy N, See H, Tran-Cong T. A spectral collocation technique based on integrated Chebyshev polynomials for biharmonic problems in irregular domains. Applied Mathematical Modelling 2009;33(1):284-299.

3. Yang C, Li X. Meshless singular boundary methods for biharmonic problems. Engineering Analysis with Boundary Elements 2015;56:39-48.

4. Pei X, Chen CS, Dou F. The MFS and MAFS for solving Laplace and biharmonic equations. Engineering Analysis with Boundary Elements 2017;80:87-93.

5. Fan CM, Huang YK, Chen CS, Kuo SR. Localized method of fundamental solutions for solving two-dimensional Laplace and biharmonic equations. Engineering Analysis with Boundary Elements 2019;101:188-197.

6. Lei M, Sam CN, Hon YC. Generalized Finite Integration Method with Volterra operator for multi-dimensional biharmonic equations. Engineering Analysis with Boundary Elements 2020;111:22-31.

7. Abbasbandy S, Shivanian E, AL-Jizani KH, Atluri SN. Pseudospectral meshless radial point interpolation for generalized biharmonic equation subject to simply supported and clamped boundary conditions. Engineering Analysis with Boundary Elements 2021;125:23-32.

8. Gupta MM, Manohar RP. Direct solution of the biharmonic equation using noncoupled approach. Journal of Computational Physics 1979;33(2):236-248.

9. Stephenson JW. Single cell discretizations of order two and four for biharmonic problems. Journal of Computational Physics 1984;55(1):65-80.

10. Mai-Duy N, Tanner RI. Computing non-Newtonian fluid flow with radial basis function networks. Int. J. Numer. Meth. Fluids 2005;48:1309-1336.

11. Ho-Minh D, Mai-Duy N, Tran-Cong T. A Galerkin-RBF approach for the streamfunction-vorticity-temperature formulation of natural convection in 2D enclosured domains. CMES: Computer Modeling in Engineering and Sciences 2009;44(3):219-248.

12. Mai-Duy N, Tran-Cong T. A compact five-point stencil based on integrated RBFs for 2D second-order differential problems. Journal of Computational Physics 2013;235:302-321.

13. Harris MF, Kassab AJ, Divo E. A shock-capturing meshless scheme using RBF blended interpolation and moving least squares. Engineering Analysis with Boundary Elements 2019;109:81-93.

14. Zhang X, Yao L. Numerical approximation of time-dependent fractional convection-diffusion-wave equation by RBF-FD method. Engineering Analysis with Boundary Elements 2021;130:1-9.

15. Cao D, Li X, Zhu H. A polynomial-augmented RBF collocation method using fictitious centres for solving the Cahn–Hilliard equation. Engineering Analysis with Boundary Elements 2022;137:41-55.

16. Zheng H, Fan Z, Li J. Simulation of electromagnetic wave propagations in negative index materials by the localized RBF-collocation method. Engineering Analysis with Boundary Elements 2022;136:204-212.

17. Mai-Duy N, Tran-Cong T. Numerical solution of differential equations using multi-quadric radial basis function networks. Neural Networks 2001; 14(2):185-199.

18. Ling L, Trummer MR. Multiquadric collocation method with integralformulation for boundary layer problems. Computers & Mathematics with Applications 2004;48(5–6):927-941.

19. Sarra SA. Integrated multiquadric radial basis function approximation methods. Computers & Mathematics with Applications 2006;51(8):1283-1296.

20. Li M, Chen CS, Hon YC, Wen PH. Finite integration method for solving multi-dimensional partial differential equations. Applied Mathematical Modelling 2015;39(17):4979-4994.

21. Mai-Duy N, Strunin D. New approximations for one-dimensional 3-point and two-dimensional 5-point compact integrated RBF stencils. Engineering Analysis with Boundary Elements 2021;125:12-22.

22. Mai-Duy N, Strunin D, Karunasena W. Computing high-order derivatives in compact integrated-RBF stencils. Engineering Analysis with Boundary Elements 2022;135:369-381.

23. Bayona V, Flyer N, Fornberg B, Barnett GA. On the role of polynomials in RBF-FD approximations: II. Numerical solution of elliptic PDEs. Journal of Computational Physics 2017;332:257-273.

24. Hoang-Trieu TT, Mai-Duy N, Tran-Cong T. Several compact local stencils based on integrated RBFs for fourth-order ODEs and PDEs. CMES: Computer Modeling in Engineering and Sciences 2012;84(2):171-203.

25. Huang C-S, Lee C-F, Cheng AH-D. Error estimate, optimal shape factor, and high precision computation of multiquadric collocation method. Engineering Analysis with Boundary Elements 2007;31(7):614-623.

26. Le-Cao K, Mai-Duy N, Tran-Cong T. An effective integrated-RBFN cartesian-grid discretization for the stream function–vorticity–temperature formulation in nonrectangular domains. Numerical Heat Transfer, Part B: Fundamentals 2009;55(6):480-502.

Table 1: Example 2: Results by the proposed 9-point stencil are much more accurate than those by the conventional 13-point stencil (Gupta and Manohar [8]) and the compact 9-point stencil (Stephenson [9]). It is noted that the IRBF approximations are all carried out with the RBF width $a = 0.001$, a tolerance in the iterative procedure is set to 10^{-14}, and $\alpha(\gamma)$ means $\alpha \times 10^{\gamma}$.

	Gupta,		Stephenson			Proposed stencil
h	Manohar	h	$O(h^2)$	$O(h^4)$	h	(IRBF8)
1/20	1.981(-2)	1/4	3.873(-4)	2.555(-5)	1/4	2.8706(-5)
		1/8	9.492(-5)	6.523(-7)	1/5	2.5461(-6)
		1/16	3.035(-6)	–	1/6	7.8680(-9)
					1/7	4.9778(-10)
					1/8	3.0615(-11)

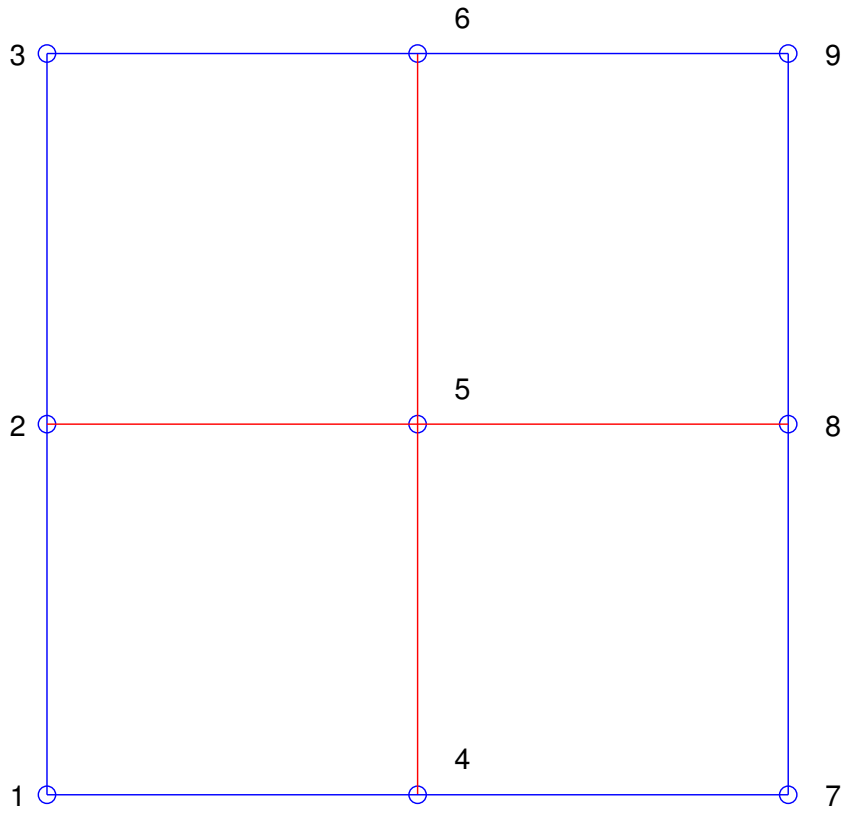

Figure 1: A 9-point stencil: The process of replacing the nodal derivative values with nodal function values involves the approximations along the two red grid lines for the variable v, and along all the grid lines of the stencil for the variable u. If the grid node is a boundary node, the associated value of the variable v can be calculated from the boundary approximation and there is no need for expressing it in terms of the nodal values of the variable u.

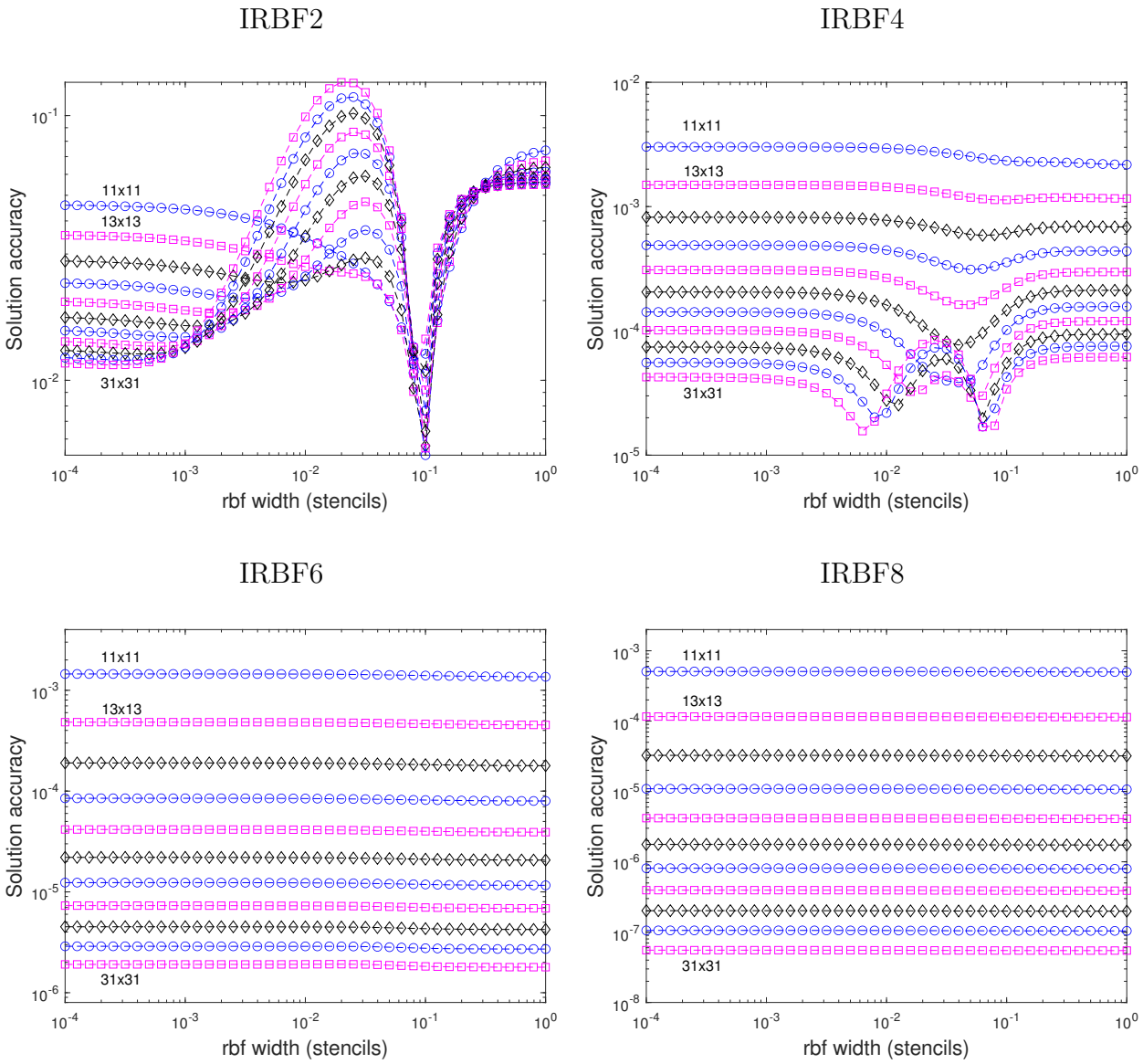

Figure 2: Example 1, $N_x \times N_y = (11 \times 11, 13 \times 13, \cdots, 31 \times 31)$: Effect of the RBF width associated with the stencil on the solution accuracy. The approximations over the stencil and along the grid lines are all carried out by using IRBF2, IRBF4, IRBF6 and IRBF8. For the approximations along the grid lines, the RBF width of 0.001 is implemented for all the four schemes. It can be seen that the IRBF solution is more accurate and less dependent on the RBF width with an increase in the order of the IRBF scheme.

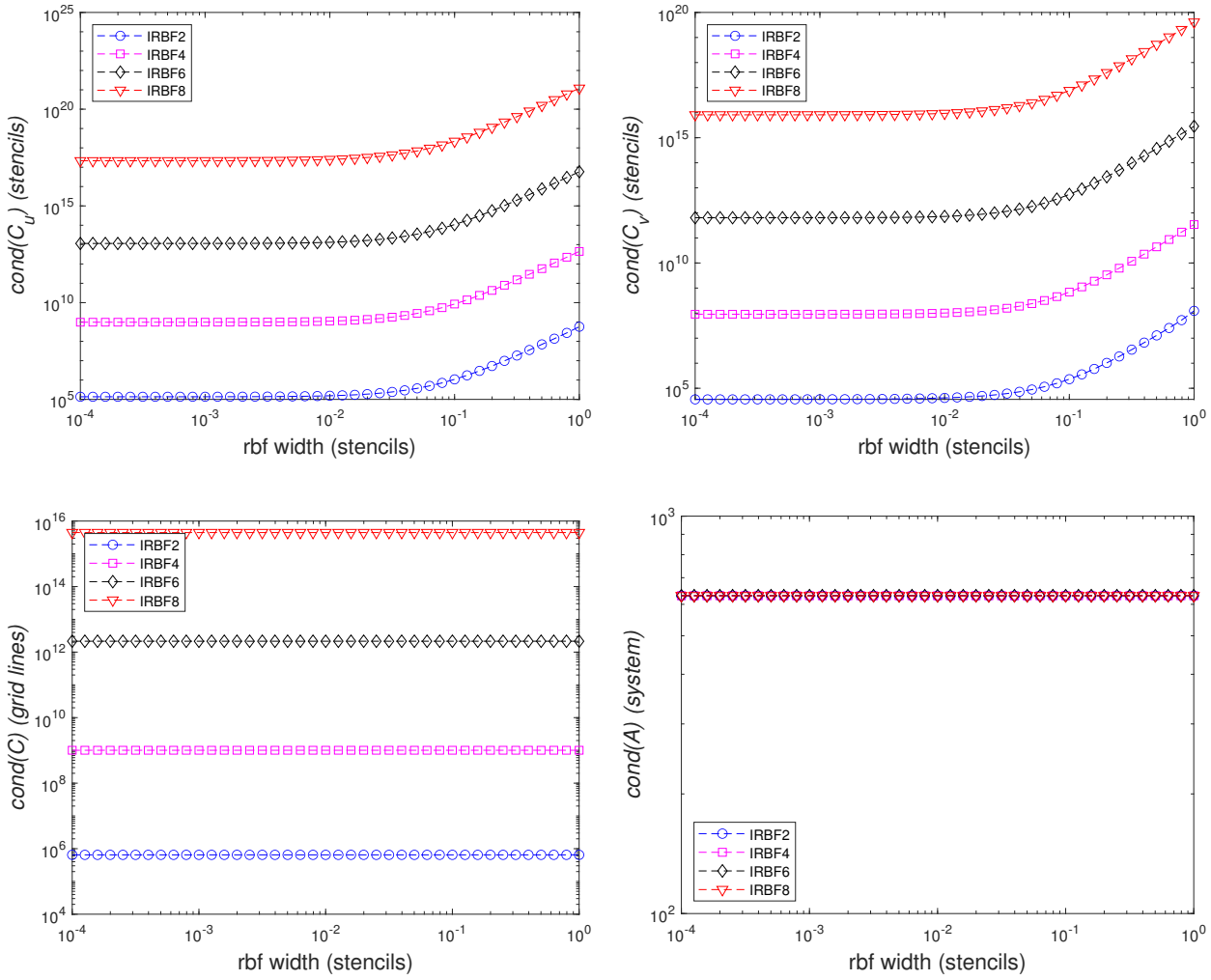

Figure 3: Example 1, $N_x \times N_x = 31 \times 31$: Effect of the RBF width associated with the stencil on the condition numbers of the conversion matrices and the system matrix. For the system matrix $\mathcal{A}$, the four IRBF schemes produce similar condition numbers, which are small (about $O(10^2)$) and stay unchanged with the RBF width. For the conversion matrices, the condition numbers are increasing functions of the RBF width. In addition, an IRBF scheme of higher order produces a larger condition number. Large global systems can be handled by standard/double precision (16-digit accuracy), while a higher level of numeric precision is needed for dealing with small local conversion systems.

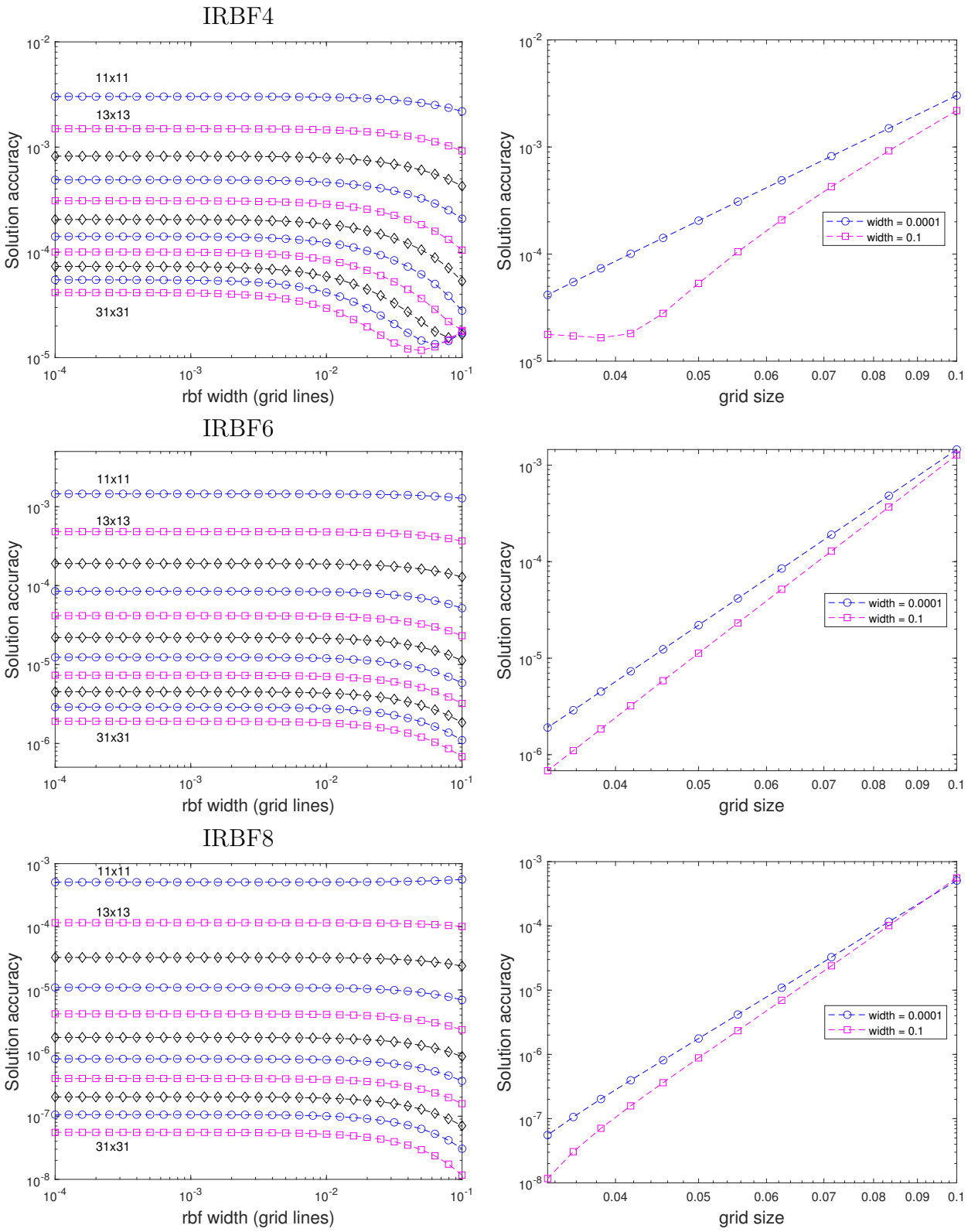

Figure 4: Example 1, $N_x \times N_y = (11 \times 11, 13 \times 13, \cdots, 31 \times 31)$: Effect of the RBF width associated with the grid lines on the solution accuracy. For the approximations on the stencil, the RBF width of 0.001 is implemented for all the schemes. The behaviours of convergence of the IRBF process at two end-points of the width range are displayed. At the left value of the range ($a = 10^{-4}$), the solution converge as $O(h^{3.89})$ for IRBF4, $O(h^{6.04})$ for IRBF6 and $O(h^{8.25})$ for IRBF8. At the right value $a = 10^{-1}$, the IRBF solution converges as $O(h^{4.85})$ for IRBF4, $O(h^{6.85})$ for IRBF6 and $O(h^{9.59})$ for IRBF8. High rates of convergence are obtained over a wide range of the RBF width. In this regard, the RBF width here does not have a strong influence on the solution accuracy.

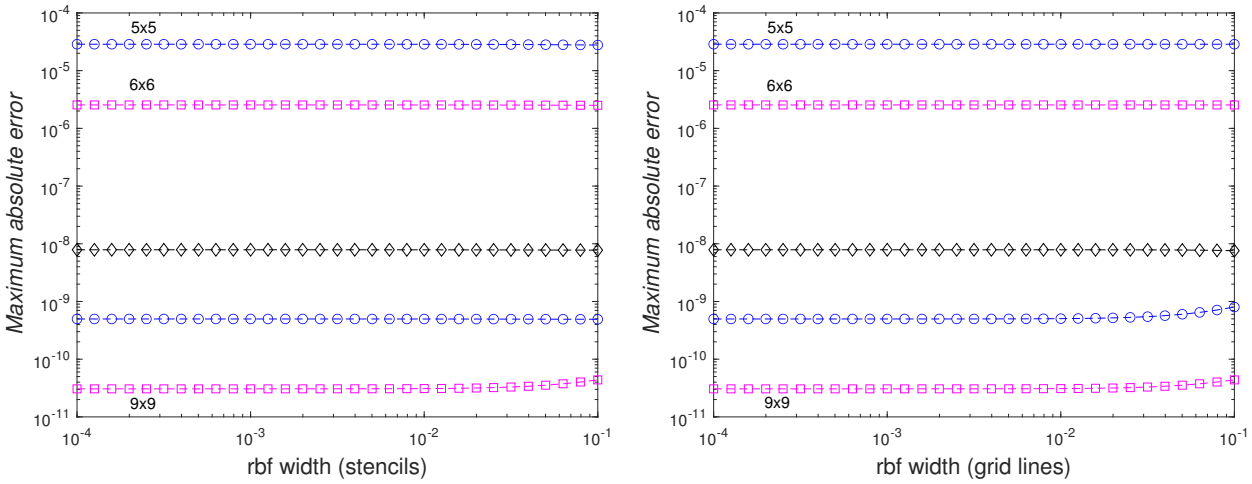

Figure 5: Example 2, $N_x \times N_y = (5 \times 5, 6 \times 6, \cdots, 9 \times 9)$, IRBF8: Effect of the RBF width associated with the stencil (left) and effect of the RBF width associated with the grid lines on the solution accuracy. The RBF solutions are not influenced much by the RBF widths. Highly-accurate results are obtained over a wide range of the RBF width.

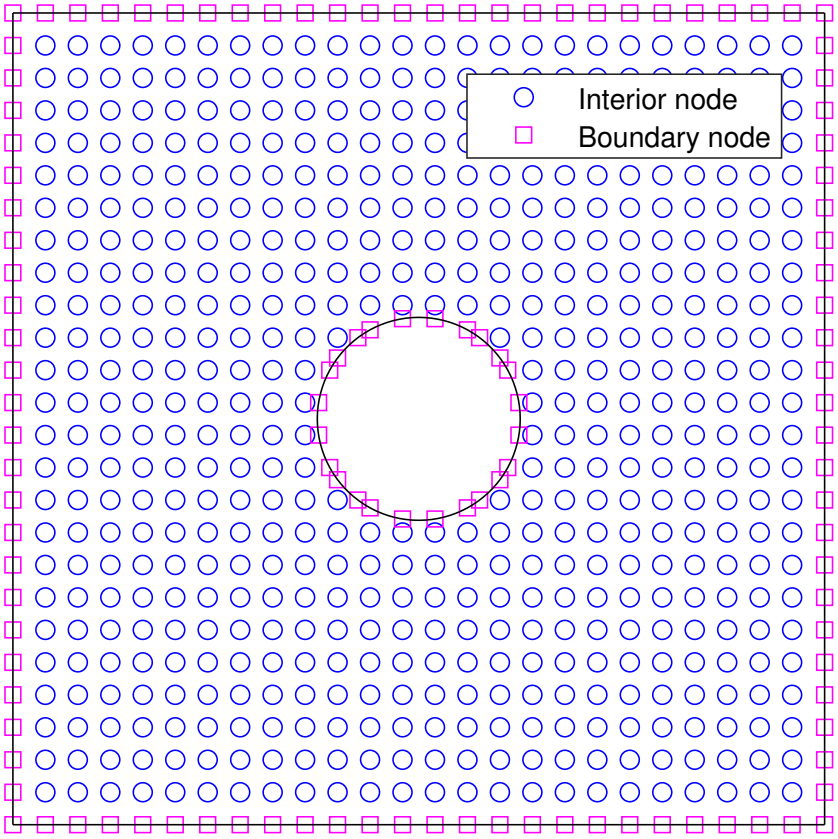

Figure 6: Domain of interest and its associated discretisation.

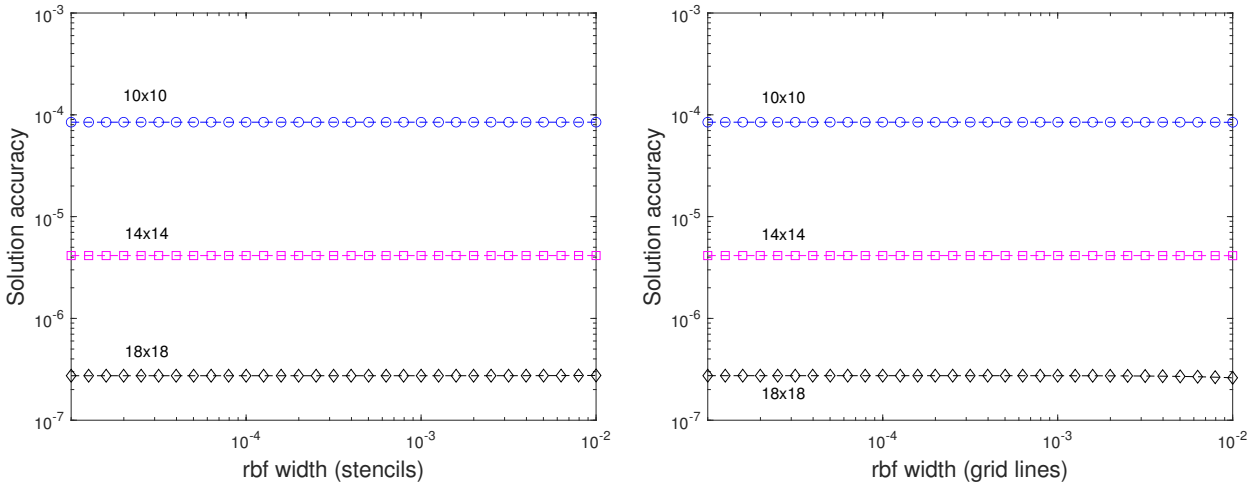

Figure 7: Example 3, non-rectangular domain, IRBF6, $N_x \times N_y = (10 \times 10, 14 \times 14, 18 \times 18)$: Effect of the RBF width associated with the stencils (left) and effect of the RBF width associated with the grid lines (right) on the solution accuracy. For the former, the RBF width used for the grid lines is set to 0.001. For the latter, the RBF width used for the stencils is also set to 0.001. The RBF solutions are not influenced by the RBF widths. The solution converges as $O(h^{8.97})$ for the left values on the right figure and $O(h^{9.03})$ for the right values on the right figure.